Computation of Propeller-Hull Interaction using Simple Body-Force Distribution Model around Series 60 C_B = 0.6

by Yan Naing Win*, *Student Member*
Ping-Chen Wu *, *Member*
Yasuyuki Toda*, *Member*
Emel Tokgoz*, *Student Member*
Frederick Stern**

Summary

The simple body-force distribution model by quasi-steady blade element theory is coupled with the Reynolds averaged Navier-Stokes (RANS) code CFDSHIP-IOWA to study the propeller-hull interaction. The ship model is Series S60 (C_B = 0.6) ship model without hub, without rudder and the propeller is a right-handed 5 blade fixed pitch Modified-AU methodical series type which is treated as infinite bladed model. Computations are performed for the ship sailing straight ahead with- and without propeller. In the without propeller case, the bare-hull results are made sure for confirmation with the experimental data to prove the magnitude of the flow field quantities with fair agreement. The computations are performed while the propeller model is working on various propeller loadings and the results of propulsive performances and flow fields in the wake regions are compared with the EFD data. Summarizing the results, the present propeller model proves its capabilities on the studies of propeller-hull interaction with much less computational effort and verifies its possibility for the load varying case.

1. Introduction

Many researches on propeller-hull interaction have been done by many researchers in past decades using different concepts of propeller model. Stern et al.[1] presented a comprehensive viscous method in which a numerical method for calculating the viscous flow over and in the wake of a ship is coupled with a propeller-performance program in an interactive and iterative manner to predict the combined flow field which is completed by Stern et al.[2] in the validation of the method. Simonsen et al.[3] presented a model that interactively determines propeller-hull interaction with a simplified potential theory-based infinite-bladed propeller model coupled with RANS code CFDSHIP-IOWA. Takada et al.[4], Kawamura et al.[5], Chou et al.[6], Tahara et al.[7], and Simonsen et al.[8] have presented different propeller models ranging from prescribed models to interactive panel models in the calculation of body-force field for the case of propeller behind the ship without rudder. In Abdel-Maksoud et al.[9], a propeller behind a ship is modeled by its real geometry.

The present research focuses on a new body-force propeller model, with a simplified quasi-steady blade element theory using the total velocity computed by CFD code, and on the interaction of it with the hull. The model is much simplified that the modeling of the real propeller geometry is not necessary and even Polar type of grid[10] or Cartesian type[11] is not a concern as it works well on both types. The inflow velocity components including induced velocity effect by time-averaged infinite bladed vortex system shed by propeller blade are determined by RANS code and thrust and torque distributions are calculated by blade element theory.

The present work mainly covers three cases: (1) a study of the flow field around the ship itself without propeller and comparison with experiment, (2) a study of the ship with the propeller model interacting each other and comparison of flow fields and propulsive performances with experiment at its self-propulsion point, and (3) a study of the ship-propeller interaction on various propeller loadings to understand the propeller performance more and to prove the ability of proposed propeller model for free-running test. All the computation results are validated with the EFD data taken from Toda et al. [12] where the ship model in the computation is represented by original offsets and the experimental model is modified to install the propeller and stern tube and propeller dummy hub were installed for without propeller condition.

In this paper, the RANS method and the grid geometry is presented briefly with the detailed explanation of blade element theory. In each section, the discussion covers the bare-hull computation and the specific analyses on the interaction between ship and propeller in terms of the propulsive performance, wake field pattern, surface-pressure and the resistance components and the corresponding information of the validation is provided. Also, the discussion for various propeller loading conditions and the availability of the present model for load varying test is provided in the last section.

* Department of Naval Architecture and Ocean Engineering, Osaka University
** IIHR - Hydro science & Engineering, the University of Iowa, Iowa City, IA, 52242, USA.

Received 26th August 2013

2. Computational fluid dynamics method

The computations are performed with the RANS solver CFDSHIP-IOWA version 4 which is an unsteady single-phase level-set solver with dynamic overset grids[13]. It solves the continuity and unsteady incompressible RANS equation (Eq. (1) and Eq. (2)) using a blended $\kappa-\varepsilon$ / $\kappa-\omega$ model for turbulence without wall-function. Captive, semi-captive, and full 6DOF capabilities for multi-objects with parent/child hierarchy are available but 6DOF function is deleted out in the present work and the computation is performed for the ship-fixed case parallelization with MPI-based domain decomposition.

$$\frac{\partial U_i}{\partial X_i}=0 \tag{1}$$

$$\frac{\partial U_i}{\partial t}+U_j\frac{\partial U_i}{\partial X_j}=-\frac{\partial \hat{p}}{\partial X_i}+\frac{1}{\mathrm{Re}}\frac{\partial^2 U_i}{\partial X_j \partial X_j}-\frac{\partial}{\partial X_j}\overline{U_i^{'}U_j^{'}}+f_{b_i} \tag{2}$$

All variables and properties are non-dimensionalized by the ship speed U_0, ship length L_{PP} and water density ρ with nomenclature: $U_i=(U,V,W)=(u/U_0, v/U_0, w/U_0)$ which is mean velocity component, $U_i^{'}$ which is fluctuation velocity, $X_i=(x/L_{PP}, y/L_{PP}, z/L_{PP})$ which is the Cartesian coordinate, $\hat{p}=(p-p_\infty)/(\rho U_0^2)+z/Fr^2$ which is piezometric pressure. f_{bi} is the body-force term representing the propeller model effect non-dimensionalized by $\rho U_0^2/L_{PP}$ and is calculated as in Eq.(13), and the Reynolds stresses related to the mean rate of strain through an isotropic eddy viscosity is calculated as in Eq.(3) where δ_{ij} is Kronecker delta and k is the turbulent kinetic energy.

$$-\overline{U_i^{'}U_j^{'}}=v_t\left(\frac{\partial U_i}{\partial X_j}+\frac{\partial U_j}{\partial X_i}\right)-\frac{2}{3}\delta_{ij}k \tag{3}$$

For the discretization strategy, second-order Euler backward difference is used for time derivatives, the convective terms are discretized by second-order upwind method and the viscous terms in momentum and turbulence equations are by second-order central difference scheme. Projection method is used for the velocity-pressure coupling.

3. Geometry and Grid Topology

The Series 60 ship model is 4.0 m long with breath, 0.533 m and mid-ship draft, 0.213m which is considered for 1 ms^{-1} speed. Based on the length and ship speed, the computation is performed at Froude's number 0.16 and Reynolds' number 3.96×10^6 which is mean value for velocity measurements. (The Reynolds' number for resistance and load varying test is different). The propeller is the MAU methodical series with 145.65-mm diameter, constant pitch with a pitch ratio 1.031, expanded area ratio of 0.7451, zero skew, 6 degree rake and 5 blades with hub ratio 0.2 and is non-dimensionalized by the ship model length. The shaft immersion ratio is 0.88.

The whole computational grid domain is comprised of totally five blocks. The boundary layer grids at the port and starboard of the ship hull are generated fine enough to capture the boundary layer flow around the solid hull surface and a very fine grid is generated for the propeller too. These grids use the O-grid topology as shown in Fig.1.

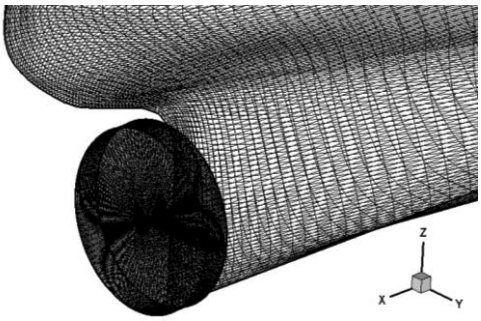

Fig.1 Ship model grid and propeller grid.

The refinement grid is used near the stern region that covers the propeller in order to capture the wake field well. The background grid is the outermost part of the grid with the finer grid spacing near the free surface and these two blocks are using H-grid topology. The computation is performed by over 6.8 million grids totally with the additional grids information shown in Table 1.

Table 1 Grid Topology and number of grids.

Block Name	Grids Type	Total Number of Grids
Background	H	3,946,536
Boundary Layer Grids (Port & Starboard)	O	2,202,200
Propeller	O	159,075
Refine	H	522,801
Total		6,830,612

The whole grid domain with boundary conditions is shown in Fig.2. The free surface is located at z/L_{pp} = 0 and 0.22L_{pp} height above the free surface is generated and water depth has one ship length-equivalent height. The boundary layer grid is shown to the port part only for the clear vision of the hull solid surface where no-slip boundary condition is applied. Apart from inlet and exit boundary condition, far field conditions are given for the bottom and top and zero gradients is given for the two sides.

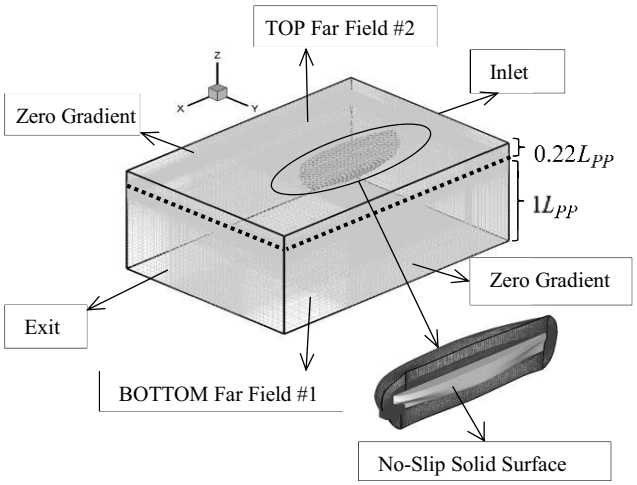

Fig.2 Grid domain with boundary conditions.

4. Propeller model

The propeller model is treated as the infinite-bladed model with a simplified quasi-steady blade element theory with consideration of time averaged propeller induced velocity field. The propeller blade has airfoil shape and twist distribution and the blade element uses these geometrical properties to determine the forces exerted by a propeller on the flow field. The propeller blade which has radius, R is split into each piece of width dr forming airfoil control volume with the radial distance r from the center of the propeller. The drag and lift forces are computed on each segment and the integration of forces along the blade gives thrust (T) and torque (Q) of the propeller.

The airfoil segment of the blade is shown in Fig.3 where OA is the zero-lift line and OB is the nose-tail line of the foil. When the propeller is rotating, in addition to the effective inflow velocity, there will be an induced velocity by the propeller and the RANS computation can give the total axial velocity component U_t, which is CD in the figure. And, when the tangential velocity with tangential induced velocity is V_θ, it will face the relative angular velocity $2\pi nr$ oppositely and the resultant tangential velocity component to the blade element is $2\pi nr - V_\theta$ which is OD in Fig.3. The resultant velocity V_R is calculated as in Eq. (4) and the hydrodynamic pitch angle (β) is calculated as in Eq. (5). Based on the geometry in Fig.3 where n is the number of revolution, the geometric pitch angle α_{g0} is calculated by $\tan^{-1}(H/2\pi r)$ where H is the pitch of the blade and the effective pitch (H_e) is achieved by $H_e = 1.08H$ in the current research. By the formula $\alpha_{g1} = \tan^{-1}(H_e/2\pi r) - \alpha_{g0}$ and $\alpha = \alpha_{g0} - \beta$, the inflow angle of attack can be calculated which is equal to $(\alpha + \alpha_{g1})$. Then, the lift coefficient can be calculated as shown in Eq. (6).

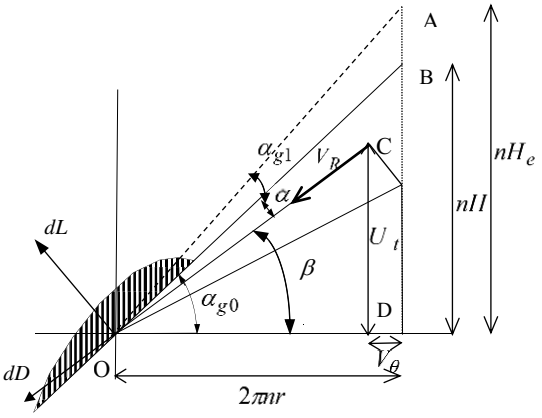

Fig.3 Concept of blade element theory.

$$V_R = \sqrt{U_t^2 + (2\pi nr - V_\theta)^2} \tag{4}$$

$$\beta = \arctan\left(\frac{U_t}{2\pi nr - V_\theta}\right) \tag{5}$$

$$C_l = 2\pi k \sin(\alpha + \alpha_{g1}) \tag{6}$$

The drag coefficient C_D is assumed to be 0.02. The variable k in Eq. (6) represents the blade-to-blade interaction effect calculating based on the maximum chord length of the blade (Eq. (7)). The segmental lift and drag forces are calculated by Eq. (8) and Eq. (9) where c is the chord length of each segment.

$$k = 1.07 - 1.05\left(\frac{c_{0.7R}}{R}\right) + 0.375\left(\frac{c_{0.7R}}{R}\right)^2 \tag{7}$$

$$dL = 0.5 C_l V_R^2 c dr \tag{8}$$

$$dD = 0.5 C_D V_R^2 c dr \tag{9}$$

The blade has a suction surface and pressure surface, and the vortices shed from the blade tips into the slip stream on the induced velocity field that can create multiple helical structures in the wake and play a major role in the induced velocity distribution. For the compensation of this deficiency, Prandtl's tip loss correction factor is deployed in the computation of thrust and torque force as shown in Eq. (10) to Eq. (12)[14].

$$F = \frac{2}{\pi}\cos^{-1} e^{-f_{tip}}, \quad f_{tip} = \frac{N}{2}\frac{R-r}{r\sin\beta} \tag{10}$$

$$dT = (dL\cos\beta - dD\sin\beta)F \tag{11}$$

$$dQ = (dL\sin\beta + dD\cos\beta)rF \tag{12}$$

The axial and tangential body-force terms are calculated as in Eq. (13) which is implemented in Eq. (2) where ΔX is the grid spacing and N is the number of blade, and Y and Z components are computed as $f_{bY} = f_{b\theta}\cos\beta$ and $f_{bZ} = -f_{b\theta}\sin\beta$. The integration of the segmental thrust and torque forces from the hub to the tip multiplied by the number of blade gives the total thrust and torque forces (Eq. (14)) where r_B is the hub radius and the corresponding thrust and torque coefficients are calculated in Eq. (15) and D is the propeller diameter.

$$f_{bX} = \frac{dT}{\Delta X}\frac{N}{2\pi r dr}, \quad f_{b\theta} = \frac{dQ}{\Delta X}\frac{N}{2\pi r^2 dr} \tag{13}$$

$$T = \int_{r_B}^{R}\int_0^{2\pi} f_{bX} r d\theta dr, \quad Q = \int_{r_B}^{R}\int_0^{2\pi} f_{b\theta} r^2 d\theta dr \tag{14}$$

$$K_T = \frac{T}{n^2 D^4}, \quad K_Q = \frac{Q}{n^2 D^5} \tag{15}$$

It is obvious that the proposed method is very simple and a comparison can be made with another simple infinite propeller model, which is a combined induced velocity by time averaged circulation distribution and the blade element theory, proposed by Kyushu University and the model is known as Yamazaki model[15]. This current method is an equivalent method in viscous flow code with Kyushu University method in potential flow theory. Within this theory, the inflow velocity components, including induced velocity effect by time averaged infinite bladed vortex system shed by propeller blade, to the propeller are determined by CFD code and thrust and torque distributions are calculated by blade element theory with some modification similar to the potential flow theory. Therefore, the potential flow code is not required in the proposed method which is simplifier[10].

5. Computation and results

5. 1 Without propeller condition

Before coupling the propeller model to the RANS code, the bare-hull itself is computed first and the flow field in the stern region especially at the propeller section is compared with the experiment to ensure the RANS result is good enough. The essential feature of the mean flow is required to predict with

considerable accuracy, including the pressure, the boundary-layer thickness and the mean-velocity field at the stern. The computation is performed for many time steps to achieve the converged solution as it will be used as the initial flow field when the propeller model is turned on. The axial velocity contour and cross-flow vector of the computation at the propeller plane x/L_{PP} =0.9875 are shown Fig.5 and Fig.8 with a comparison to the EFD flow field. The wake field in this section is analyzed to confirm that the nominal wake inflow is reliable to work with a propeller model. The flow field at this section is important as the thrust and torque of the propeller will be calculated based on it. In the cross-flow vector field shown in Fig.8, the experimental vector is a bit longer than that of CFD because the effect of stern tube displacement and modification of the cursor stern shape in EFD makes the cross-flow fields higher.

When the ship is towed without propeller, the pressure field is high near the stern region, making an additional forward force which is consequently reduced the resistance. So, the surface-pressure for bare-hull case is required to make a comparison with the case of with-propeller conditions to observe the effect of propeller. The bare-hull resistance is computed by the combination of the components of friction, pressure and wave and the non-dimensional data shows 0.343×10^{-3} which is 0.2% lower than the experimental data, 0.344×10^{-3} and the comparison is illustrated in Fig. 20. It shows the present computation shows good agreement with experimental data.

5. 2 Convergence history and propulsion performance

When the computation is performed with the propeller, the primary concern is to get good agreement with EFD data at its self-propulsion point so that the propeller revolution rate is firstly fixed at model point n=7.8 rps with advance coefficient based on ship speed $J_s = 0.88$. In the computation, the propeller model is run for every time step and there are 3 to 5 internal iterations in each time step. For the prevention of computational divergence, the amount of body-force which is treated in momentum equation is controlled by means of relaxation factor which is given by a small amount of 0.1 at the beginning and when the thrust and torque coefficient is converged in the specific time-steps, it is increased by an interval 0.1 and the procedure continues until the relaxation factor becomes 1. The computation at full relaxation factor is continued until the thrust and torque coefficients are converged.

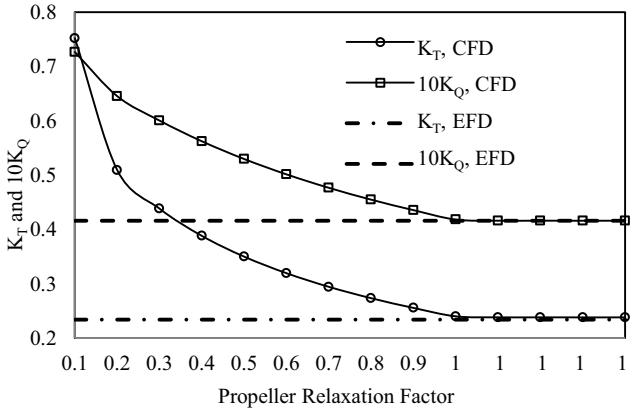

Fig.4 Convergence history of thrust and torque.

The interactive procedure between the RANS solution and propeller-performance program is unnecessary for this model and the convergence history of the thrust and torque is shown in Fig.4. When the propeller starts working in the undisturbed wake, the thrust and torque coefficients are quite high and then decrease gradually as it runs more continuously because the propeller works harder in the undisturbed nominal wake field than in the effective wake. The final converged thrust and torque coefficients are 0.238 and 0.0416, both of which overpredict a little bit.

Table 2 Comparison with EFD and previous propeller models.

Propeller Model	Thrust Coefficient	Torque Coefficient
	K_T	$10K_Q$
EFD	0.234	0.411
Vortex Lattice Method (by Stern et al.[2])	0.231	0.399
Kyushu University Model (by Simonsen et al.[3])	0.257	0.435
Blade Element Theory (Present work)	0.238	0.416

The results are compared with not only the EFD data as well as the other two previous models of Stern et al.[2] and Simonsen et al.[3] at the same advanced coefficient to understand the performance capability of the proposed propeller model more and these are summarized in Table 2. It shows that the closer results are obtained for both K_T and K_Q than Kyushu University Model. For comparing with Vortex Lattice Model, the similar results are obtained. In the present case and other two previous models, the original bare hull is used instead of the modified hull with stern tube and the dummy hub, so more detailed discussion is not shown here.

The effective wake factor is calculated as in Eq. (16), where w is the wake fraction, on the basis of a thrust identity and J_a is obtained from the open water characteristics curve of the same propeller using the same model by Togkoz et al.[10] based on the advanced speed as $J_a = U_a / nD$ and J_s is corresponding to the thrust measured when the propeller is running behind the ship based on the ship speed as $J_s = U_s / nD$.

$$(1-w) = \frac{J_a}{J_s} \tag{16}$$

The effective wake factor of the current work is 0.73 which is a little bit lower than EFD which shows 0.75 and this underprediction would make sense as the thrust is overpredicted. More discussions on wake fraction and the thrust deduction factor which is related to the resistance forces and thrust are described in the last section of this paper based on various propeller loadings to understand the nature of the propeller better.

5. 3 Flow field

The flow field in the wake region which is the combination of potential, viscous and the wave wake is much complicated to manipulate and the propulsion performance is much dependable on the nature of the wake. The propeller will not give right amount of thrust in the incorrect wake field and it is important to

use a propeller model, which is located in the wake, to give right amount of suction on the upstream as well as right velocity distribution to the downstream for the rudder. In this paper, the wake region without propeller is validated first with EFD data with good agreement. For proving the proposed new propeller model is working well, the wake field including the velocity components fields U,V,W as well as pressure coefficient C_P when the ship and propeller are working together is needed to analyze in detail not only on the upstream of the propeller but also on the downstream and should get closed agreement with the experimental result.

In the current case, the propeller is located at x/L_{PP} =0.9875 and the flow field is studied at x/L_{PP} =0.98125 in upstream region and at x/L_{PP} =1.0 for downstream. The axial velocity contour and cross-flow vectors comparison with EFD is plotted for each location as shown in Fig.5 to Fig.10. In the upstream region, the velocity contour as well as the cross-flow vector shape shows good agreement with EFD though there is no stern tube in the computation. Analyzing the downstream part will give clear understanding of the flow nature of the propeller. At this section, the maximum axial velocity shape of 1.2 (Fig. 7) is much closed to the experimental result and it shows better result than that of Stern et al.[2] and Simonsen et al.[3] where the maximum axial velocity space is narrower than EFD. The cross-flow vector field for the downstream part is also plotted and compared with EFD and the good agreement is achieved. As the downstream region is mostly influenced by the effect of the presence of propeller, the flow nature at far downstream sections are also analyzed which are available through the authors.

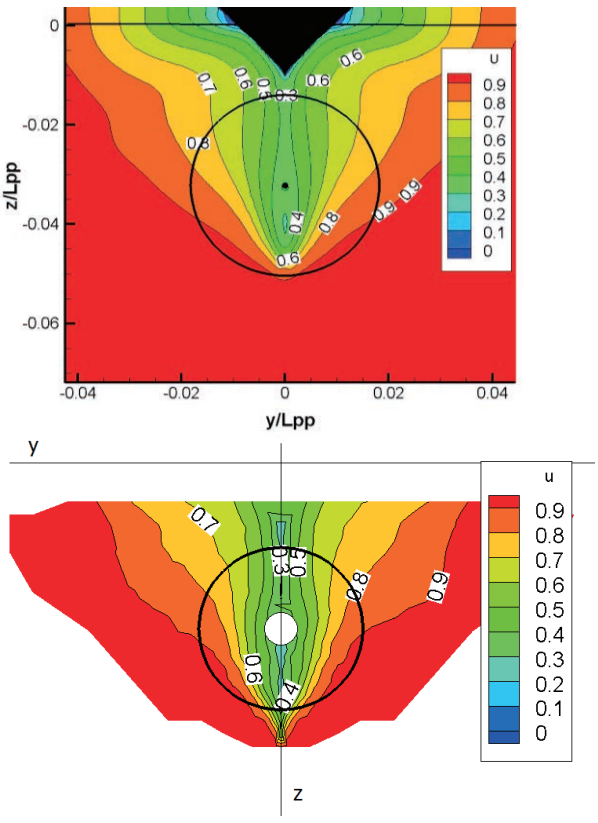

Fig.5 Comparison of axial-velocity contours at x/L_{pp} = 0.9875 between CFD (upper) and EFD (lower) (Without-propeller condition).

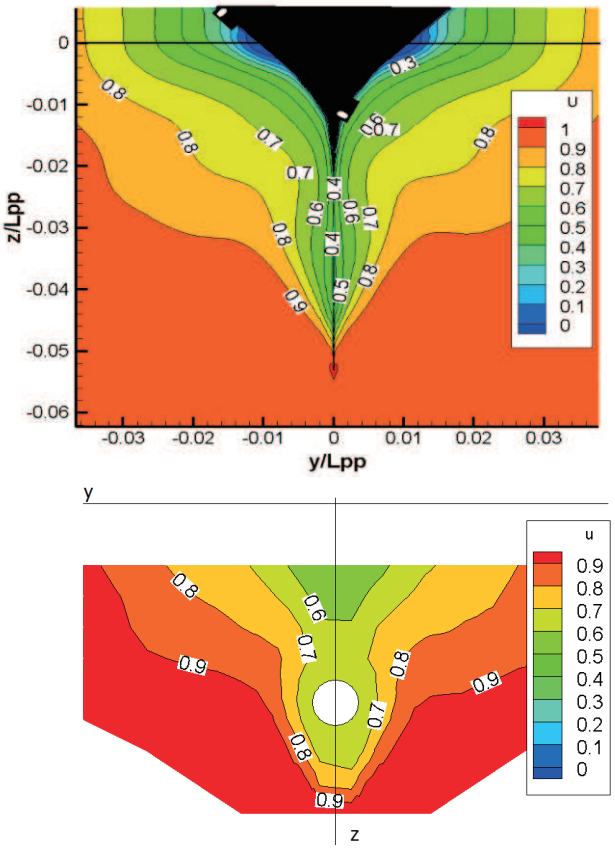

Fig.6 Comparison of axial-velocity contours at x/L_{pp} = 0.98125 between CFD (upper) and EFD (lower) (With-propeller condition).

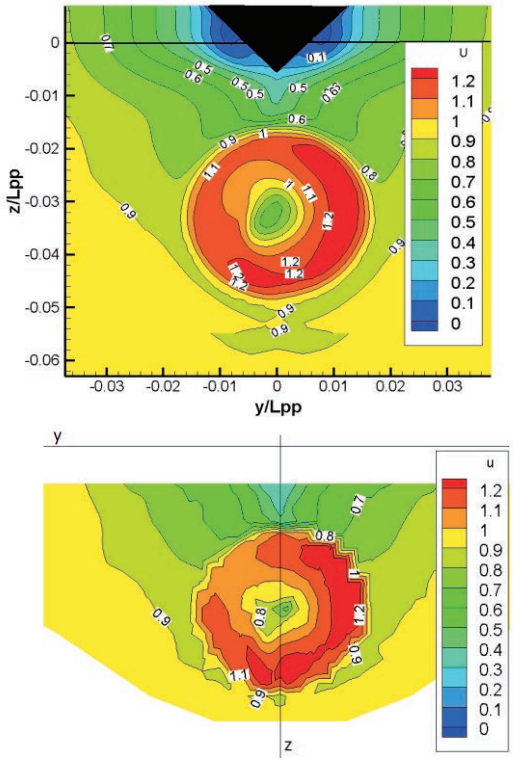

Fig.7 Comparison of axial-velocity contours at x/L_{pp} = 1 between CFD (upper) and EFD (lower) (With-propeller condition).

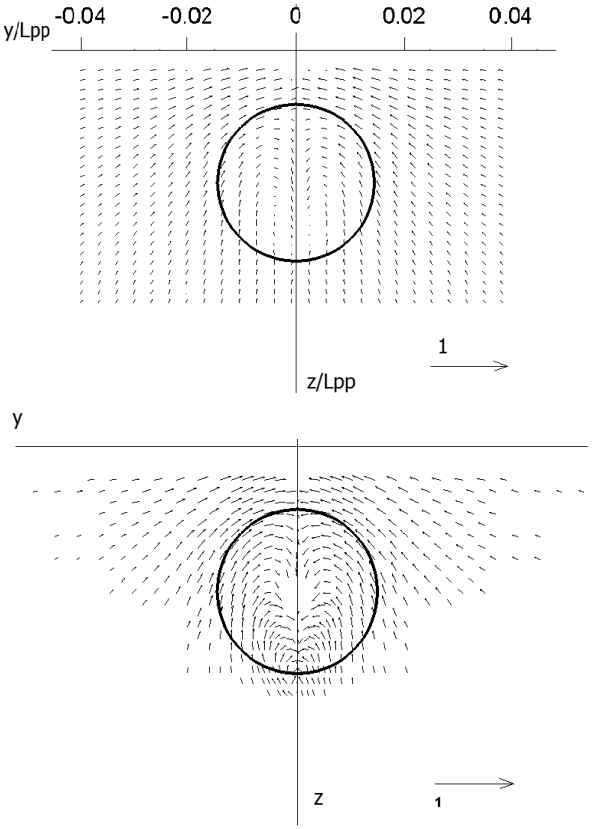

Fig.8 Comparison of cross-flow vectors at x/L_{pp} = 0.9875 between CFD (upper) and EFD (lower) (Without-propeller condition).

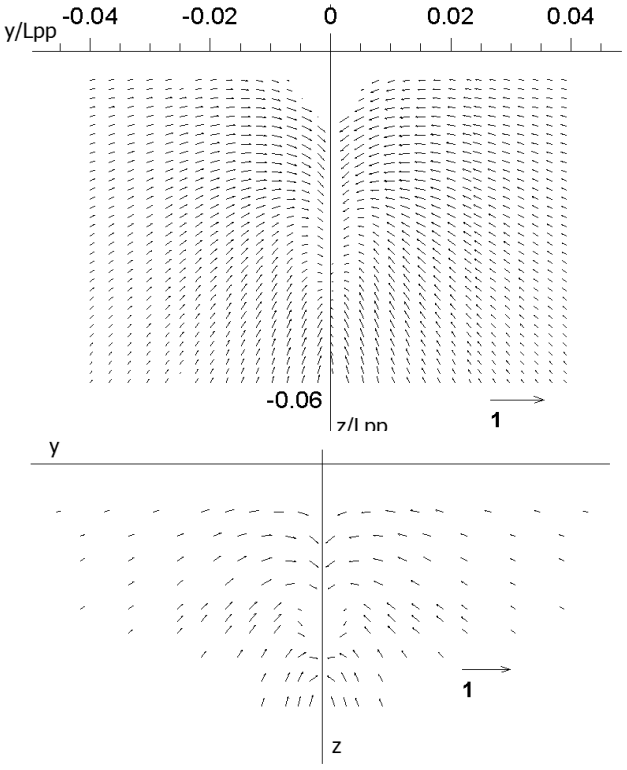

Fig.9 Comparison of cross-flow vectors at x/L_{pp} = 0.98125 between CFD (upper) and EFD (lower) (With-propeller condition).

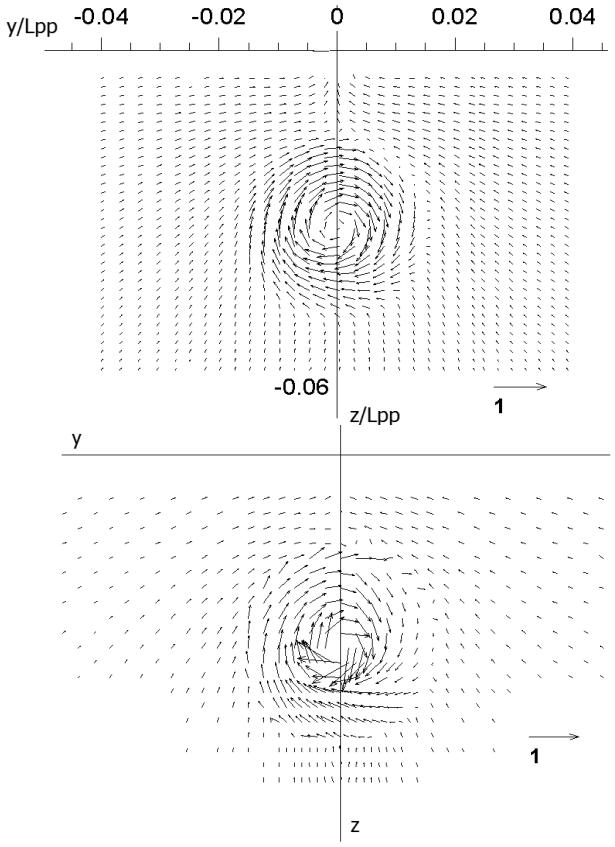

Fig.10 Comparison of cross-flow vectors at x/L_{pp} = 1 between CFD (upper) and EFD (lower) (With-propeller condition).

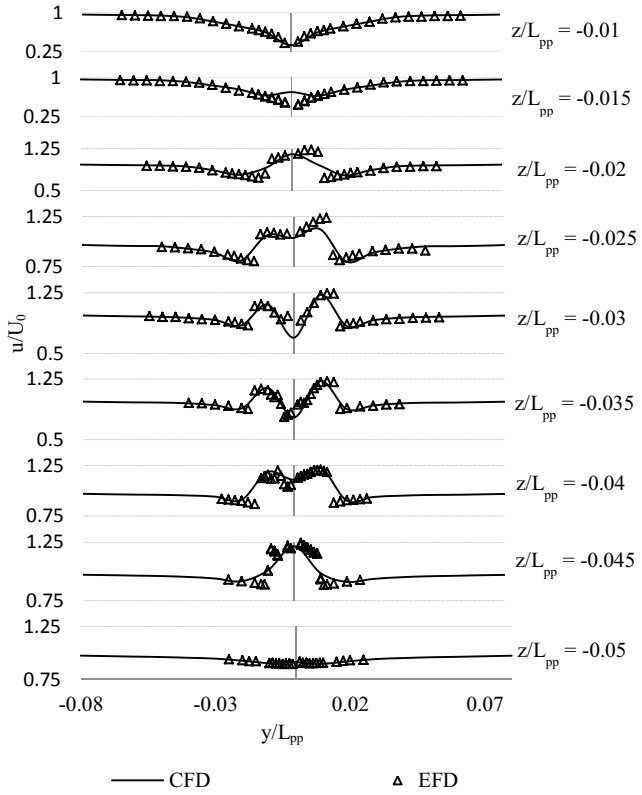

Fig.11 Comparison of U between CFD and EFD at x/L_{pp} = 1.0 (With-propeller condition).

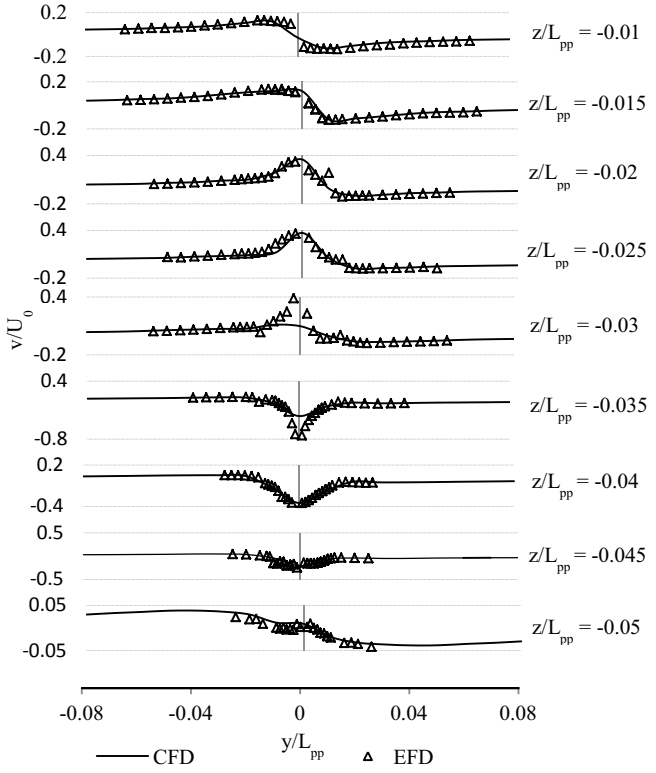

Fig.12 Comparison of V between CFD and EFD at x/L_{pp} = 1.0 (With-propeller condition).

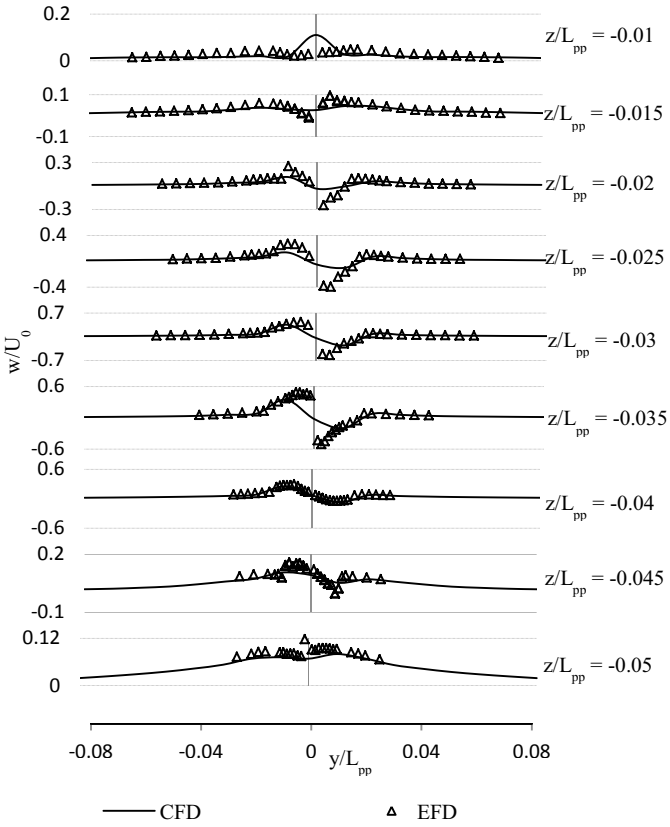

Fig.13 Comparison of W between CFD and EFD at x/L_{pp} = 1.0 (With-propeller condition).

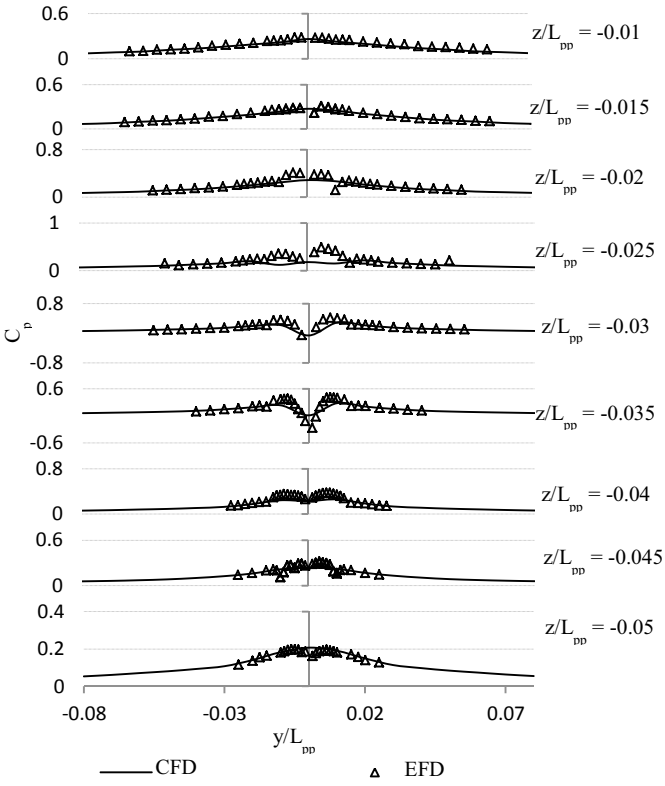

Fig.14 Comparison of C_p between CFD and EFD at x/L_{pp} = 1.0 (With-propeller condition).

The detailed flow field analyses are plotted comparatively with EFD data at each section ranging $-0.05 \le z/L_{PP} \le -0.01$ shown in Fig.11 to Fig.14. The axial-velocity fields give good agreement generally but, for cross-flow velocity components in downstream, in EFD results, large cross-plane velocity components are observed near the center plane due to the lack of strong hub vortex in CFD because the hub and boss cap are neglected i.e. V and W components are lower than experiment. The pressure field of the computation gives lower near the center line because of the lack of the stern tube. Generally, the computation result gives good agreement.

Fig.15 and Fig.16 show the difference in axial-velocity contours between the with- and without-propeller conditions Δu for regions upstream at x/L_{PP} =0.98125 and downstream of the propeller at x/L_{PP} =1. For upstream part, Δu is larger near the center plane of the hull in regions of low momentum fluid where the flow undergoes largest axial acceleration. For downstream part, Δu has the effect of propeller body force and large Δu is observed because of the accelerated flow behind the propeller and the largest is near the hull center plane. Δu is generally large in the starboard side than the port side due to the tangential component of the hull wake. Δu is studied for each z/L_{PP} section with EFD data. At z/L_{PP} =0.02, as it is still near the hull, the boundary layer is thick and Δu shape is broad whereas for z/L_{PP} =0.045, the boundary layer is thin and Δu is narrow, peaked. Generally, most of the data trends are similar to the EFD data with a bit lower Δu near the center plane.

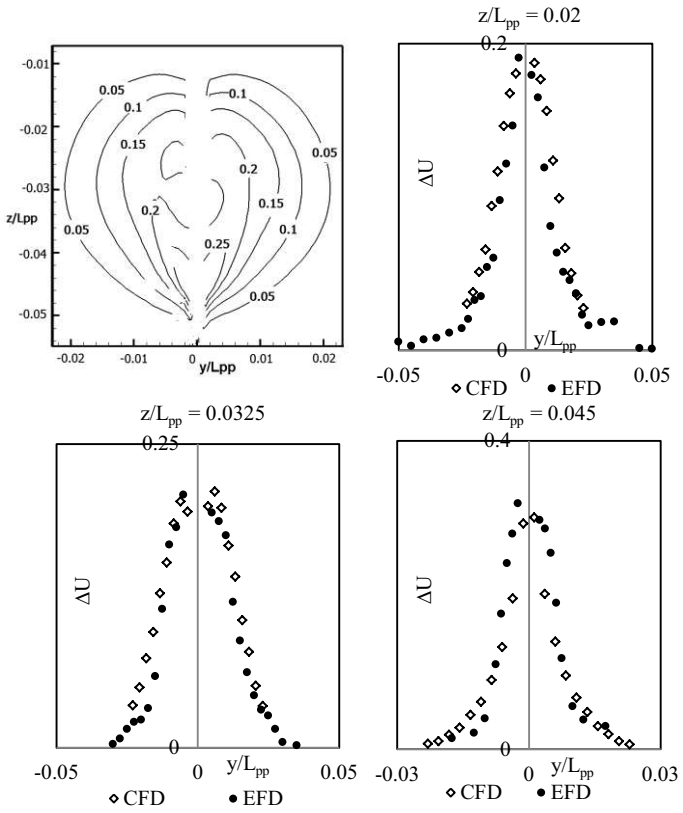

Fig.15 Axial-velocity difference Δ*u* between the with- and without-propeller conditions for upstream of propeller.

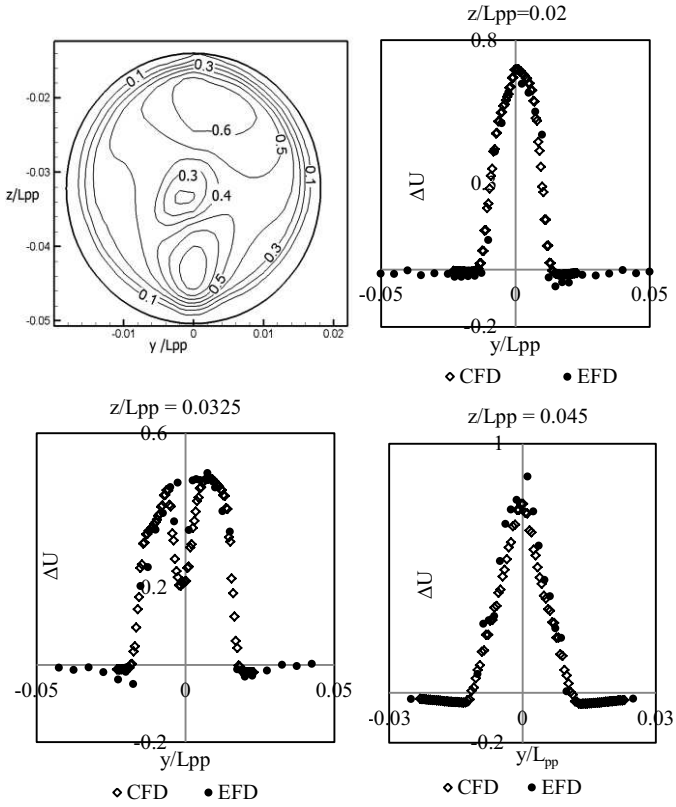

Fig.16 Axial-velocity difference Δ*u* between the with- and without-propeller conditions for downstream of propeller.

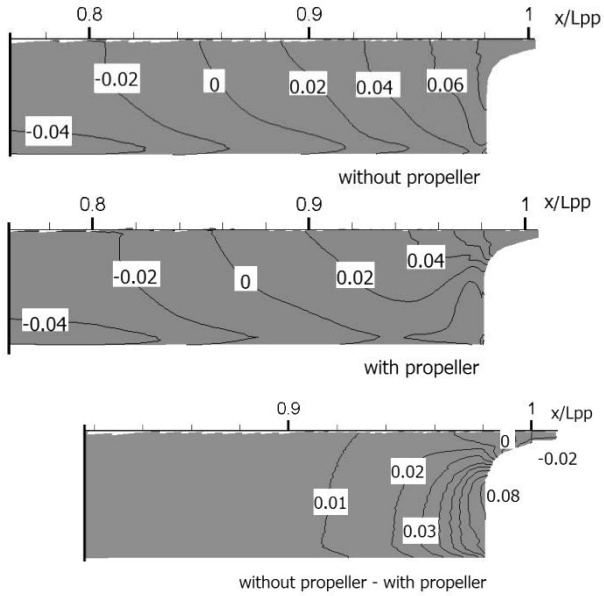

Fig.17 Surface-pressure distributions: pressure contours.

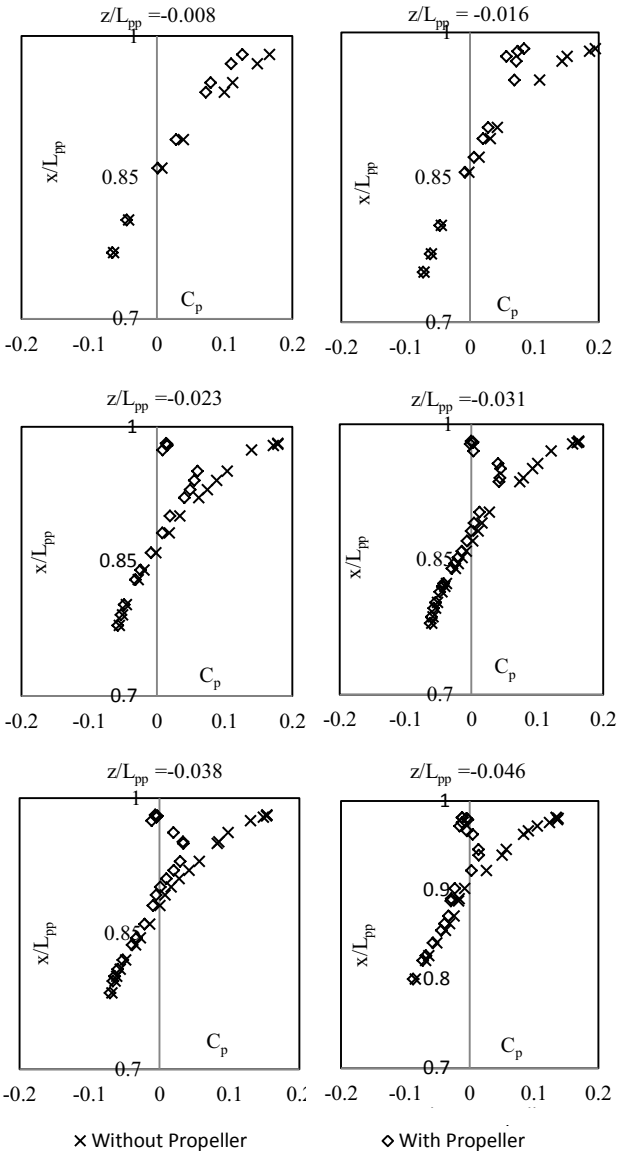

Fig.18 Surface-pressure distribution: stream-wise variation.

The surface-pressure contour near the stern is an interest to know the effect of propeller. Similar to the description in section 5.2, the high pressure region near the stern of the hull without propeller is reduced by the interaction of propeller behind the ship. This behavior is clearly shown in Fig.17. The high pressure contour level in without-propeller condition becomes somewhat lower in with-propeller case. As the stern tube is lack in the hull, the pressure contour at the end of the stern is different with EFD where the negative pressure occurs in the above and positive pressure in the below of the stern tube due to the boundary layer effect[12]. The pressure difference is computed by subtracting the with-propeller from the without propeller and that explains the propeller effect on the hull. The surface pressure is plotted at each z/L_{PP} section along the hull at the stern region in Fig.18, comparing the data between with and without propeller conditions and the propeller effect is distinctly clear to see. The surface pressure of the port and starboard side are similar so that only port side data are illustrated in both Fig. 17 and Fig.18.

5. 4 Prediction for free-running capability

The propeller model is computed for fixed number of revolution, the propulsion quantities as well as the flow field is studied in comparison with EFD data and the validation is proved with good agreement in previous section. The proposed propeller model becomes an interesting tool to use for load varying test which is mostly treated in present by the axisymmetric prescribed body-force method based on the Hough and Ordway circulation distribution[16]. To check this capability, the propeller is necessary to rotate on various numbers of revolutions from low loading to higher loadings continuously with the precise configuration of the thrust and torque force.

In current work, the advanced coefficients based on ship speed J_s are set at 1.05 (6.5 rps), 1.02 (6.7 rps), 0.93 (7.4 rps), 0.88 (7.8 rps) and 0.87 (7.9 rps) of which 0.88 case is computed and proved in the above sections. So, the other four cases are computed similarly starting from the converged nominal solution of bare-hull and using the body-force relaxation factor as a control function and the computation is performed until the thrust and torque coefficients are converged. These results are plotted in Fig.19 and the comparison of the result is shown in Table 3.

Table 3 Propulsive quantities at various loadings.

J_S	CFD		EFD	
	K_T	$10K_Q$	K_T	$10K_Q$
1.05	0.189	0.358	0.182	0.345
1.03	0.196	0.367	0.189	0.350
0.93	0.225	0.401	0.215	0.394
0.88	0.238	0.416	0.234	0.411
0.87	0.242	0.420	0.233	0.421

In load-varying test, the propeller is turned on at low number of revolution which is then increased to higher loading gradually and the computation is required to be able to handle the case with accurate estimation of the thrust and torque while the loading is increased. So, firstly, the propeller is set to run at J_s=1.05 until converged, then, the number of revolution is increased gradually in each time step in a small interval and computed until J_s=0.85 and the result is represented by line illustration in Fig.19. Surprisingly, the line passes all dotted points that mean the propeller can predict the right thrust and torque while the loading is increasing gradually. So, the proposed propeller model has a capability to work for load varying test even with the side forces by the inflow velocity components of V and W[10] that is restricted in the axisymmetric body-force model which is widely used for load varying test these days.

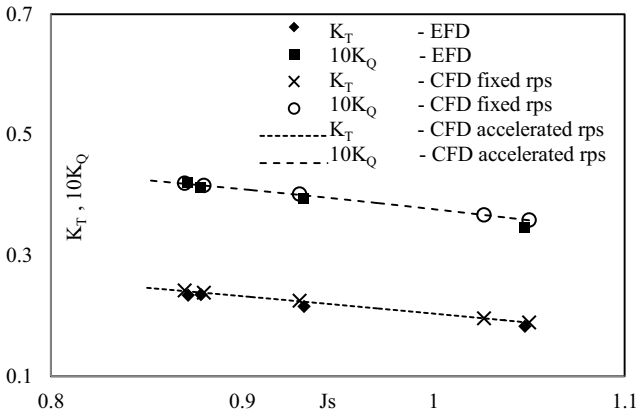

Fig.19 Propulsive quantities on various propeller loadings.

Fig.20 shows the total resistance on various propeller loadings comparing with the experiment. The bare-hull resistances of CFD and EFD are plotted at T = 0 with good agreement. In EFD, the resistance forces are a bit higher than the bare-hull resistance that is the effect of the inclusive of propeller which makes the pressure in the stern region lower and increase the total resistance. The higher the loadings are, the higher the total resistance is. In CFD, the similar slope is observed where the value is lower than EFD. It is reasonable to explain this feature as hub and cap are neglected in the computation that means there is blank region in the hub and some of the flow passes through this place while the propeller is working and that phenomenon reduces the total resistance. When the hub geometry is included with the propeller, this effect will be disappeared. Because of this effect, the thrust deduction factor is a bit hard to compute. But, the two slopes of resistance forces are similar and the propeller is evident at its good working ability. The wake fraction based on loading coefficient C_T, $C_T = 2T/\pi^2$ is shown in Fig.21 and all values are lower than EFD data as the propeller overpredicts at all cases in Table 3.

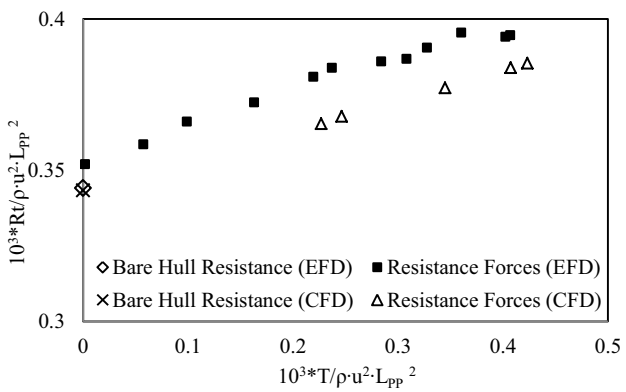

Fig.20 Total resistance forces comparison.

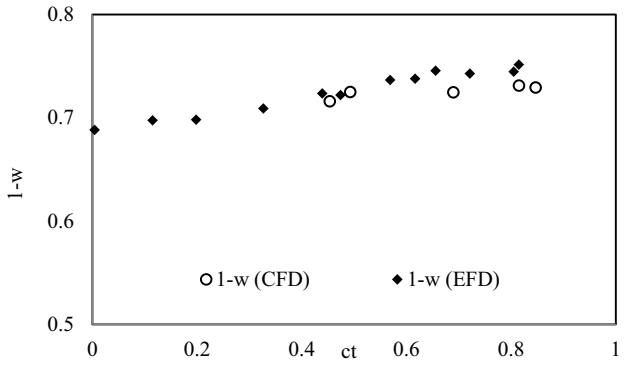

Fig.21 Effective wake factor comparison of CFD and EFD.

6. Conclusions

A new propeller model with blade element theory is coupled with RANS computation code to study the interaction between the hull and propeller without requiring detailed modeling of propeller geometry and unnecessarily required to choose polar grid or Cartesian grid for the propeller. Before implementing the propeller model, the flow around the bare-hull itself is computed and the flow field near the wake regions is observed, discussed and validated. The computation is performed on various propeller loadings and the discussion is focused mainly on the experimental model point at n=7.8 rps. A lot of researches are performed by many authors in this case and the comparison is made not only with the EFD data but also with some previous models. The computation results are interpreted, discussed and some weak facts are discovered for avoidance in future research like the lack of hub geometry. The computation results on various propeller loadings are also discussed and proved the capability for free-running test with corresponding comparison with the EFD data. The total resistance forces and the wake fractions are plotted based on thrust loading coefficients and the behavior of the propeller is observed.

As a conclusion, closed agreements have been proved with the experiment confirming the ability of the proposed propeller model and assuring its eligibility for load varying test, various maneuvering tests and ship-ship interaction case for extensive research field by overcoming the restrictions of the propulsion capability in the computation field presently. In overall, the proposed propeller model with the real hub geometry will be a significant useful tool for the computation in propulsion researches.

Acknowledgment(s)

This work was partially supported by JSPS KAKENHI Grant Number 24246142. The authors of this research give their heartily thanks to Dr. Hamid Sadat-Hosseini, an assistant research scientist at the University of Iowa, Iowa City, IA, USA.

References

1) Stern, F., Kim, H. T., Patel, V. C., and Chen, H. C.: A viscous-flow approach to the computation of propeller-hull interaction, Journal of Ship Research, Vol. 32, No.4, pp. 263-284, 1988.

2) Stern, F., Kim, H.T., Zhang, D.H., Toda, Y., Kerwin, J. and Jessup, S.: Computation of Viscous Flow Around Propeller-Body Configurations: Series 60 CB = 0.6 Ship Model, Journal of Ship Research, Vol. 38, No.2, pp. 137-157, 1994.

3) Simonsen, C.D. and Stern, F.: RANS Maneuvering Simulation of Esso Osaka with Rudder and a Body-Force Propeller, Journal of Ship Research, Vol. 49, No. 2, pp. 98-120, 2005.

4) Takada, N., and El Moctar, O. M.: Simulation of viscous flow about "Esso Osaka" in maneuvering motion, Proceedings, 3rd Numerical Towing Tank Symposium, Tjarno, Sweden, September, 2000.

5) Kawamura, T., Miyata, H., and Mashimo, K.: Numerical simulation of the flow about self-propelling tanker models, Journal of Marine Science and Technology, 2, 245-256, 1997.

6) Chou, S.K., Chau, S.W., Chen, W.C., and Hsin, J. Y.: Computations of ship flow around commercial hull forms with free surface or propeller effects, Proceedings, Workshop on Numerical Ship Hydrodynamics, Gothenburg, Sweden, 2000.

7) Tahara, Y., and Ando, J.: Comparison of CFD and EFD for KCS container ship in with/without propeller conditions, Proceedings, Workshop on Numerical Ship Hydrodynamics, Gothenburg, Sweden, 2000.

8) Simonsen, C.D., and Cross-Whiter, J.: Study of three RANS body-force propeller models, Proceedings, 5th Numerical Towing Tank Symposium, Pornichet, France, 2002.

9) Abtel-Maksoud, M., Rieck, K., and Menter, F. R.: Unsteady numerical investigation of the turbulent flow around the container model (KCS) with and without propeller, Proceedings, Workshop on Numerical Ship Hydrodynamics, Workshops on Numerical Ship Hydrodynamics, Gothenburg, Sweden, September, 2000.

10) Tokgoz, E., Win, Y. N., Kuroda, K. and Toda, Y.: A New Method to Predict the Propeller Body Force Distribution for Modeling the Propeller in Viscous CFD Code without Potential Flow Code, 2nd East Asia International Student Symposium on Maritime Sciences, Kobe, Japan, 4 pp., 20-24 November 2012.

11) Yokota, S.: The simple prediction method for body-force distribution in CFD code, B.S. Thesis (In Japanese), Osaka University, 2013.

12) Toda, Y., Stern, F., Tanaka, I. and Patel, V.C.: Mean-flow measurements in the boundary layer and wake of a series 60 CB = 0.6 model ship with and without propeller, IIHR Report No. 326, Iowa Institute of Hydraulic Research, The University of Iowa, Iowa City, 1988.

13) Paterson, E. G., Wilson, R. V., and Stern, F.: General-purpose parallel unsteady RANS ship hydrodynamic code: CFDSHIP-IOWA, *IIHR report No. 432*, 2003.

14) Shen, W.Z., Sorensen, J.N. and Mikkelsen, R.: Tip Loss Correction for Actuator/Navier-Stokes Computations, Journal of Solar Energy Engineering, Vol. 127, pp.209-213, 2005.

15) Yamazaki, R.: On the Propulsion Theory of Ships on Still Water (Improved Theoretical Method), Memoirs of the Faculty of Engineering, Kyushu University, Vol. 34, No.1, pp. 65-88, 1977.

16) Hough, G. and Ordway, D.: The generalized actuator disk, *Tech. Report TAR-TR 6401*, Therm Advanced Research, Inc., Ithaca, New York, 1964.